03.1

# Problems of flow separation detection by pressure sensors on a unmanned aerial vehicles with a propeller

© P.A. Polivanov[1,2], A.A. Sidorenko[1]

[1] Khristianovich Institute of Theoretical and Applied Mechanics, Siberian Branch, Russian Academy of Sciences, Novosibirsk, Russia
[2] Novosibirsk State Technical University, Novosibirsk, Russia
E-mail: polivanov@itam.nsc.ru

*Received July 2, 2021*
*Revised October 2, 2021*
*Accepted October 25, 2021*

An experimental study of pulsations characteristics of the zone of flow separation arising at a small airplane-type UAV with a pushing two-blade propeller were carried out. The measurements were done in wind tunnel by unsteady pressure sensors and microphones built into the skin of the UAV for the test cases with and without a rotating propeller. A significant effect of the propeller on the level of pulsations was found. An increase of the incoming flow velocity led to a weakening of this effect. Analysis of the spectral data of the disturbances did not reveal a direct relationship between the propeller noise and the unsteady characteristics of the separation zone.

**Keywords:** UAV, flow separation, unsteady pressure sensor, propeller

DOI: 10.21883/TPL.2022.02.53578.18946

The rapid progress in design of unmanned aerial vehicles (UAVs) in recent years opens up wide opportunities for aerodynamic experimentation in the field. Such UAVs serve as a versatile platform for experimental studies into inter-related issues of aerodynamics and flight mechanics and allow one to obtain large amounts of data at a reasonable cost. On the other hand, flight modes and flow control techniques used for small UAVs may be inapplicable in regular aviation [1,2]. First and foremost, post-stall flow regimes with well-developed unsteady separation flow around the wing and other elements of UAVs of an airplane configuration are examined here. Deep dynamic stall, which is potentially useful for landing on short sites, cables, or vertical surfaces [3,4], is one of the examples of such flight modes. The flight of a small UAV in turbulent atmosphere (e.g., in urban areas) is also associated with stalling and flow separation [5]. In view of this, the issue of detection of flow separation on lifting surfaces of UAVs based on the readings of certain sensors assumes great importance. Pressure sensors are the most likely candidates for this role, since they are small-sized, have relatively low power consumption figures, and are well-protected from environmental hazards.

However, their readings are very hard to interpret. In addition to not being directly sensitive to the fact of flow separation (in contrast, e.g., to shear stress sensors), such sensors and their readings are affected by the individual specifics of flow around a UAV, the laminar-to-turbulent transition [6], and other factors. Two approaches are considered in most studies. In the first one, flow separation is identified by monitoring the deviation of readings of local sensors from the pressure distribution typical of attached flow [7,8]. In the second approach, the presence of pressure pulsations (related to the emergence of unsteady separation flow) or their correlation caused by large-scale structures in separation flow [9,10] are regarded as the criteria of flow separation. If a UAV is propeller-powered, the propeller noise may both hinder the interpretation of readings of pressure pulsation sensors and affect directly the state of the boundary layer and the related formation of separation flows [11]. The study of propeller noise features fairly prominently in current UAV research [12,13], but the issue of influence of this noise on the formation of separation flows has been overlooked. The aim of the present study is to determine the effect of a propeller on the readings of unsteady pressure sensors and microphones in UAV flight modes with and without flow separation.

Experiments were performed in the T-503 wind tunnel at the Aircraft Faculty of the Novosibirsk State Technical University at flow velocity $U = 5-20$ m/s and temperature $T = 290-295$ K. This wind tunnel is a closed-type facility with an open 2 m-long circular test section with a diameter of 1.2 m. The experimental model was mounted on a three-component strain-gage balance positioned on the angle of attack mechanism of T-503 A ZOHD Nano Talon Evo small UAV was the experimental model (Fig. 1). This off-the-shelf solution has an advantage in that it offers an opportunity for rapid transition from wind-tunnel tests to flight tests, which are planned to be performed in the future. The design of ZOHD Nano Talon Evo was updated to mount it on the strain-gage balance.

Four pressure pulsation sensors and three small-sized electret microphones were installed in the UAV. Differential pressure sensors 1 INCH D1-P4V-MINI with a response time no more than 0.1 ms and a measurement range of 250 Pa were used in the experiments. VS4011S36 sensors with a frequency range of $50-10\,000$ Hz and a diameter of 4 mm were used as microphones. Pressure sensors were installed within the wing and the center body. A

pneumatic line with a length no greater than 2 cm provided the connection to an aperture on the surface of the model. Three sensors were positioned at the leeward side of the wing, and another one was positioned at the center body. Their coordinates were $Z/L = 0.27,\ 0.13,\ -0.27,\ 0.03$ (Fig. 1, *b*) and $X/b = 0.57,\ 0.57,\ 0.57,\ 0.41$, respectively. Here, $L$ is the wing span (860 mm), and $b$ is the wing root chord (170 mm). The origin of coordinate $Z$ is at the symmetry plane, and the origin of $X$ is at the leading wing-root edge. One microphone was located close to the second pressure sensor ($Z/L = 0.13,\ X/b = 0.57$) and was mounted flush with the surface. The other two microphones were positioned at the center wing. Data were recorded with an LCard E-502 analog-to-digital converter at a sampling rate of 100 kHz, the measurement duration was 5 s.

Measurements with unsteady pressure sensors were performed alongside with balance tests. The angle of attack varied from $-5$ to 19° in these experiments. Measurements were performed with both increasing and decreasing angles of attack to examine the issues of flow hysteresis. The results of balance tests revealed no hysteresis in the dependences of the lift coefficient and the drag coefficient on the angle of attack. The maximum lift-to-drag ratio was 4.5 at a flow velocity of 5 m/s and 8.5 at 15–20 m/s. These values were achieved at an angle of attack varying within the 6–9° range. The stall angle of attack varied within the 14–15° range depending on the incoming flow velocity. The lift magnitude decreased smoothly in the post-stall range of angles of attack.

When the electric motor rotating the propeller with a speed of 200 Hz was turned on, no significant changes in

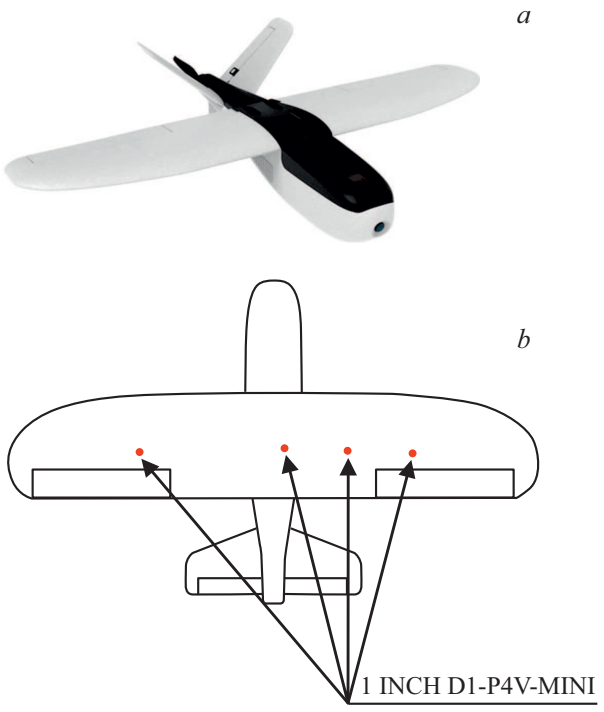


**Figure 1.** *a* — photographic image of a ZOHD Nano Talon Evo small UAV; *b* — schematic diagram of arrangement of pressure sensors on the model.

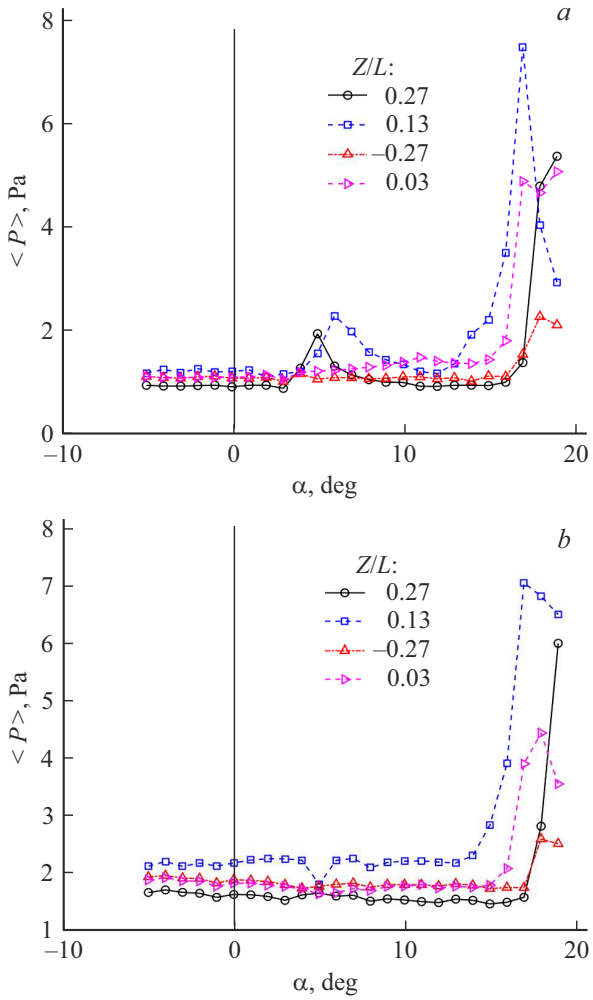


**Figure 2.** Dependence of the level of pressure pulsations on the angle of attack at $V = 10$ m/s. *a* — without the propeller, *b* — the propeller speed is 200 Hz.

the distribution of the lift coefficient with the angle of attack occurred. This indicates that the propeller noise does not have any substantial effect on the average characteristics of flow around the UAV.

Example dependences of the root-mean-square level of pressure pulsations (in the range up to 5 kHz) without the propeller on the angle of attack are presented in Fig. 2, *a*. It is evident that the most pronounced intensification of pulsations occurs when the angle of attack approaches the stall value („separation“ peak of pulsations). The level of pulsations in the region of attached flow varies weakly with a peak at 5–10°. The emergence of this pulsation peak for sensors located at the wing may be attributed to the laminar-to-turbulent transition in the boundary layer in the vicinity of a sensor („turbulent“ peak of pulsations). Additional thermal-imaging measurements confirm this assumption. The data from sensors located at the center body and near it reveal an earlier onset of growth of perturbations. This is indicative of local flow separation at the high-drag body or near it. The data provided by microphones revealed similar trends, but the level of pulsations at pre-stall angles of attack

was higher. This may be attributed to the higher sensitivity of microphones in the high-frequency part of the spectrum and the greater effect of the turbulent boundary layer on their readings. It can be seen from Fig. 2 that the data from sensors located symmetrically with respect to the UAV symmetry plane ($Z/L = 0.27$ and $-0.27$) do not match. The wing is fabricated from expanded polypropylene. The use of this material reduces the UAV cost, but makes precise fabrication of structural components impossible. Therefore, it is likely that the mentioned data mismatch is induced by a certain difference in geometry between the left and right wing panels.

Changes in the incoming flow velocity resulted in the following (not shown in the figures): as the flow velocity decreased, the amplitudes of „separation“ and „turbulent“ peaks of pulsations grew closer to each other; when the flow velocity increased, the ratio of amplitudes of „separation“ and „turbulent“ peaks also increased.

Fig. 2, *b* presents similar data obtained with the propelling plant operating at a propeller speed of 200 Hz. A change in the shape of curves is evident. The level of pulsations in the region of attached flow increases, and the „turbulent“ peak of pulsations vanishes at a velocity of 10 m/s.

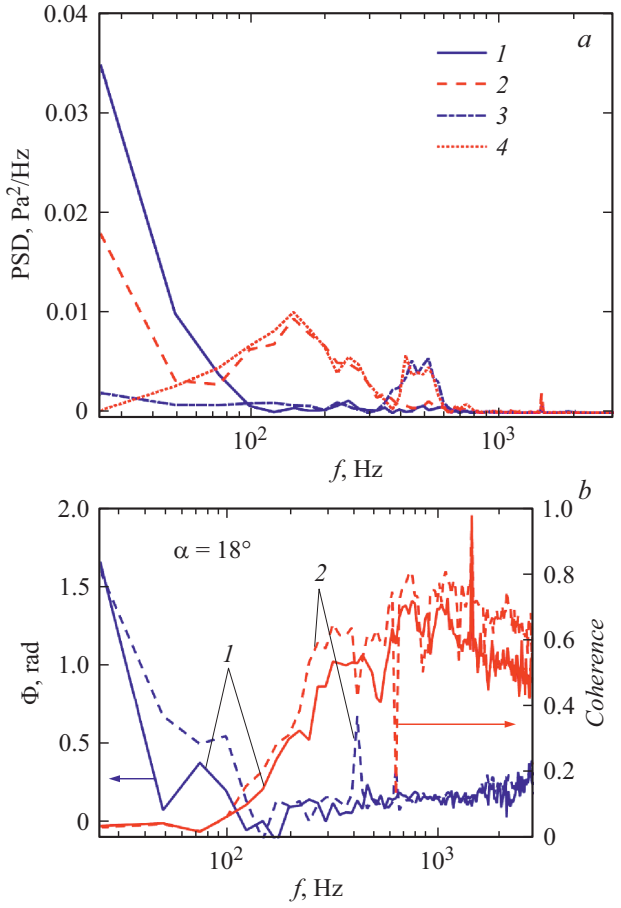


**Figure 3.** Distributions of the pressure pulsation power spectra for $Z/b = 0.27$ (*a*) and the spectra of coherence and phase difference between the sensors located at $Z/b = 0.27$ and 0.13 (*b*) obtained at $V = 10$ m/s. *1* — without the propeller, $\alpha = 18°$; *2* — the propeller speed is 200 Hz, $\alpha = 18°$; *3* — without the propeller, $\alpha = 5°$; *4* — the propeller speed is 200 Hz, $\alpha = 5°$.

As the flow velocity grows from 10 to 20 m/s, the distributions of the root-mean-square level of pulsations obtained with and without the propeller become closer to each other.

Example pressure pulsation power spectra obtained with and without the propeller for a flow velocity of 10 m/s are presented in Fig. 3, *a*. The spectra in this figure were measured at two angles of attack (5 and 18°) corresponding to attached flow and fully developed separation flow. Without the propeller, the increase in angle of attack from 5 to 18° translates into an intensification of pulsations at frequencies below $f = 100$ Hz (or, in a dimensionless form, below $\mathrm{St} = bf/V = 1.7$). This is indicative of the fact that these pulsations are associated with the separation flow. In addition, the pulsation peak in the region of 500 Hz is suppressed at an angle of attack of 18°. This pulsations peak is probably associated with oscillation of pressure due to laminar-to-turbulent transition at an angle of attack of 5°. When the propelling plant was turned on, additional pulsations in the frequency range of 100–400 Hz with their maximum around $f = 170$ Hz ($\mathrm{St} \approx 2.9$) became clearly visible at both angles of attack. In the case of separation flow, the level of pulsations at frequencies below 100 Hz decreased relative to the data obtained without the propeller. No significant variations of parameters of the peak of pulsations with characteristic frequency $\mathrm{St} \approx 2.9$ were found in the analysis of pulsation spectra for other angles of attack (not shown here). Since the data from microphones agree qualitatively with the readings of pressure sensors, they are not discussed in the present study.

The growth of pulsations with characteristic frequency $\mathrm{St} \approx 2.9$ may be attributed to noise produced in the interaction between the propeller and vortex structures developing in the shear layer at the UAV fuselage. The fuselage shape may induce local separations that form strong coherent structures. Moving downstream, these structures interact with the propeller. This interaction may produce high-power broadband acoustic noise. A change in the flow velocity translates into changes in the frequency and amplitude characteristics of the additional pulsation peak emerging in experiments with the propeller. The suppression of pulsations in the low-frequency region ($\mathrm{St} < 1.3$) in Fig. 3, *a* may be related to the rearrangement of separation flow due to the propeller noise.

The obtained data indicate that it is hard to predict the influence of a propeller on the unsteady characteristics of separation flows. Root-mean-square and spectral measurement data are evidently not sufficient for analysis of the unsteady flow structure around a UAV with a rotating propeller (e.g., in flight tests).

Owing to the complex nature of flow, additional pulsations induced by a propeller may emerge at frequencies that do not correspond to the propeller speed. The analysis of coherence spectra may help resolve the issue of interrelation between pulsations. For example, the

velocity of propagation of coherent structures formed in separations is low and close to the flow velocity. The propagation velocity of the propeller noise (sound velocity) is significantly higher. Therefore, the resulting phase delay of acoustic perturbations is significantly lower than the phase delay from unsteady structures in the separation region. Example coherence spectra between two sensors located at the wing are presented in Fig. 3, *b*. It can be seen that the signals are highly coherent in the high-frequency region ($> 400$ Hz). This is likely attributable to the fact that sensors are subjected to one and the same electric noise. At the given angle of attack, the mentioned frequency region contains almost no useful signal, and the electric noise is probably of one and the same nature. The coherence of signals deteriorates in the region of pulsations related to flow separation ($< 100$ Hz). The increase in phase delay is evident in this region. No significant phase delays are seen in the region of the additional peak induced by the rotating propeller ($100-400$ Hz). This is attributable to the fact that the phase velocities of large-scale separation structures are low (close to the flow velocity). Thus, phase delay data may be used to find the frequency range of pressure pulsations associated with separation coherent structures. The low level of coherence in the region of the useful signal is attributable to the large distance between sensors.

The obtained results reveal a significant influence of a propeller of a small UAV on the readings of unsteady pressure sensors. This should complicate further the interpretation of their readings in flight tests.

### Acknowledgments

The authors would like to thank the „Mechanics“ Joint Access Center for providing the equipment for experiments.

### Funding

The study was supported by grant 20-49-08006 of RSF.

### Conflict of interest

The authors declare that they have no conflict of interest.

## References

[1] S. Sekimoto, K. Fujita, K. Fujii, in *AIAA Science and Technology Forum and Exposition (AIAA Scitech 2021 Forum)* (AIAA, 2021), AIAA 2021-1944. DOI: 10.2514/6.2021-1944

[2] A.A. Sidorenko, A.D. Budovsky, B.V. Postnikov, I.D. Zverkov, B.Yu. Zanin, V.V. Kozlov, A.A. Maslov, Tech. Phys. Lett., **36** (4), 304 (2010). DOI: 10.1134/S106378501004005X.

[3] C. Greatwood, A. Waldock, T. Richardson, Aerospace Sci. Technol., **71**, 510 (2017). DOI: 10.1016/j.ast.2017.09.034

[4] S.H. Mathisen, K. Gryte, T.I. Fossen, T.A. Johansen, in *AIAA Infotech @ Aerosp Conf.* (San Diego, California, USA, 2016), AIAA 2016-0512. DOI: 10.2514/6.2016-0512

[5] D. Williams, V. Quach, W. Kerstens, S. Buntain, G. Tadmor, C.W. Rowley, T. Colonius, in *47th AIAA Aerospace Sciences Meeting including The New Horizons Forum and Aerospace Exposition* (Orlando, Florida, USA, 2009), AIAA 2009-143. DOI: 10.2514/6.2009-143

[6] A.V. Popov, R.M. Botez, M. Labib, J. Aircraft, **45** (1), 23 (2008). DOI: 10.2514/1.31488

[7] D. Yeo, E.M. Atkins, L.P. Bernal, W. Shyy, in *AIAA Atmospheric Flight Mechanics Conf.* (Minneapolis, Minnesota, USA, 2012), AIAA 2012-4416. DOI: 10.2514/6.2012-4416

[8] R.A. Bunge, A.E. Alkurdi, E. Alfaris, I. Kroo, in *AIAA Flight Testing Conf.* (Washington, USA, 2016), AIAA 2016-3652. DOI: 10.2514/6.2016-3652

[9] M. Marino, S. Ravi, S. Watkins, in *28th Congress of the International Council of the Aeronautical Sciences* (*ICAS 2012*) (Brisbane, Australia, 2012), vol. 2, p. 955. http://www.icas.org/ICAS_ARCHIVE/ICAS2012/PAPERS/972.PDF

[10] A. Mohamed, S. Watkins, A. Fisher, M. Marino, K. Massey, R. Clothier, J. Aircraft, **52** (3), 827 (2015). DOI: 10.2514/1.C032805

[11] V.V. Kozlov, V.N. Lushin, B.Yu. Zanin, in *Separated flows and jets*, ed by V.V. Kozlov, A.V. Dovgal (Springer, Berlin–Heidelberg, 1991), p. 525. DOI: 10.1007/978-3-642-84447-8_70

[12] A. Cambray, E. Pang, S.A. Showkat Ali, D. Rezgui, M. Azarpeyvand, in *2018 AIAA/CEAS Aeroacoustics Conf.* (Atlanta, Georgia, USA, 2018), AIAA 2018-3450. DOI: 10.2514/6.2018-3450

[13] N. Intravartolo, T. Sorrells, N. Ashkharian, R. Kim, in *55th AIAA Aerospace Sciences Meeting* (Grapevine, Texas, USA, 2017), AIAA 2017-2019. DOI: 10.2514/6.2017-2019